Carbon Dots Enhanced Graphene Field Effect Transistors for Ultrasensitive Detection of Exosomes

Sami Ramadan, [#,*] *Richard Lobo,†* *Yuanzhou Zhang,* [#] *Lizhou Xu,* [#,*] *Olena Shaforost,* [#] *Deana Kwong Hong Tsang,* [#] *Jingyu Feng,†* *Tianyi Yin,* [#] *Mo Qiao,†* *Anvesh Rajeshirke,* [#] *Long R Jiao,* [††] *Peter K.Petrov,* [#] *Iain E.Dunlop,* [#] *Maria-Magdalena Titirici,†* *and Norbert Klein*[#]

[#] Department of Materials, Imperial College London, London, SW7 2AZ, UK.

†Department of Chemical Engineering, Imperial College London, South Kensington Campus, London SW7 2AZ, U.K.

††Department of Hepatobiliary Surgery, Division of Surgery & Cancer, Imperial College London, Hammersmith Hospital Campus, Du Cane Road, London, W12 0NN, UK.

*Corresponding Authors: Dr. Sami Ramadan (s.ramadan@imperial.ac.uk); Dr. Lizhou Xu (l.xu@imperial.ac.uk)

Abstract

Graphene field-effect transistors (GFETs) are suitable building blocks for high-performance electrical biosensors, because graphene inherently exhibits a strong response to charged biomolecules on its surface. However, achieving ultralow limit-of-detection (LoD) is limited by sensor response time and screening effect. Herein we demonstrate that the detection limit of GFET biosensors can be improved significantly by decorating the uncovered graphene sensor area with carbon dots (CDs). The developed CDs-GFET biosensors used for exosome detection exhibited higher sensitivity, faster response and three orders of magnitude improvements in the LoD compared with nondecorated GFET biosensors. A LoD down to 100 particles/μL was achieved with CDs-GFET sensor for exosome detection with the capability for further improvements. The results were further supported by atomic force microscopy (AFM) and fluorescent microscopy measurements. The high performance of CDs-GFET biosensors will aid the development of an ultrahigh sensitivity biosensor platform based on graphene for rapid and early diagnosis of diseases.

Keywords: Graphene, carbon dots, field-effect-transistor, limit-of-detection, exosome, cancer diagnosis

1 Introduction

Electrical biosensors based on field-effect-transistors (FETs) have emerged as one of the most promising platforms for rapid, ultrahigh sensitive and selective detection of a wide range of biomolecules.[1] Among many FET biosensor types, graphene-FET biosensors (GFET sensors) are especially suitable as biosensors:[2] As a one-atom thick carbon layer the active volume exhibits a very high surface-to-volume ratio which offers a unique potential for high sensitivity. GFETs are highly conductive and are biologically compatible with various biomolecules such as proteins, antibodies and DNAs. In addition, the surface of graphene can be directly functionalized with biomolecules *via* physisorption or π–π interfacing while preserving its sp2 network.[3] Furthermore, large scale production of large-area graphene can be readily accomplished using techniques such as chemical vapour deposition (CVD).[4, 5] GFET sensors have been employed for the rapid and high sensitivity detection of various biological species and disease biomarkers, including DNA,[6, 7] proteins,[8] glucose,[9] viruses,[10-12] bacteria,[13] cardiovascular disease biomarkers,[14] cancer biomarkers[15, 16] and extracellular vesicles.[17] Although a GFET is able to respond to single molecules at its surface, the main challenge is associated with the mass transport of analytes to the sensor surface. In the diffusion regime, the detection of 1 fM of analyte on a planar sensor may require an incubation period of a few hours,[18, 19] which is impractical. Moreover, the surface energy of the substrate underneath the graphene might strongly affect the stability and formation of the electrical double layer (EDL).[20] This could influence the interaction between graphene and biomolecules such as proteins and antibodies and their orientation and conformation on the graphene surface.[21, 22] In addition, the instability of the EDL may affect the absorption of analytes at the sensor surface.[23, 24] All of these phenomena can reduce the capture efficiency of analytes at the graphene sensor surface, and degrade the effective sensitivity and the limit-of-detection (LoD). Therefore, the enhancement of the capture efficiency of biomolecules at the graphene surface is crucial in order to exploit graphene's capability to achieve high sensitivity and ultralow LoD.

The use of surface nanostructuring has been reported to increase the accessibility of DNA to the electrochemical sensor surface, consequently improving the capture efficiency and sensitivity of the sensor.[25, 26] Moreover, it has been suggested that diffusion towards a spherical and cylindrical nanosensor surface may be much faster than that towards a planar surface.[18, 27] Therefore, it is expected that the deposition of spherical like nanoscale objects such as carbon dots (CDs) on

graphene can act as antenna for a graphene sensor and increase capturing rates without affecting the structural properties of graphene.

CDs have shown significant promise due to their excitation-dependent fluorescence, low toxicity and biocompatibility for biosensing[28] and bioimaging.[29] They have numerous facile synthesis routes,[30] are tunable[31] and easily passivated or modified with different bioactive molecules.[32] While CDs having a wide range of potential properties, those being hydrothermally synthesised tend to have a mostly amorphous carbon core and abundant oxygen functional groups which confer strong negative surface charge.[33] These properties enable CDs particles to facilitate a valuable surface modification of graphene complementing many of the positive aspects of GFETs including high surface area-to-volume ratio.

There is increasing evidence that exosomes (small extracellular vesicles) released from cancer cells contain disease-specific information which can be used as biomarkers for diagnosis even at an early stage.[34, 35] Here in this work we show that CDs modification on GFETs greatly enhance the efficiency of exosome capture for exosome detection by improving sensitivity and the LoD of graphene biosensors. We demonstrate an enhancement of the detection performance of GFET biosensors by three orders of magnitude through this surface modification strategy. Exosomes range in size between 40–150 nm and are released by healthy and tumour cells *via* the endocytic pathway which enables cell-to-cell communication and cargo transfer.[34, 36]

2 Results and Discussion

Figure 1a shows the schematics of a GFET biosensor for exosome sensing. After the S/D metal contact deposition CDs were incorporated in the devices using drop-casting before surface functionalization. The role of CDs in increasing the sesnsitivty of the GFETs is illustrated in Figure 1b,c. It is expected that CDs on graphene modulate the electrical double layer and decrease the screening of exosome while the structure and morphology of the CDs enhance the capturing efficiency of exosome. X-ray photoelectron spectroscopy (XPS) was performed to assess the elemental composition of CDs and reveals the presence of C1s and O1s with carbon bands at 284.8 eV (C-C), 286.21 eV (C-O), 287.03 eV (C=O) and 288.68 eV (COOH), where C-C bonds forms 75% of the C1s (Figure 2a). As shown in the HRTEM image in Figure 2b, the CD particles exhibit

size between 5-10 nm. Their height distribution on graphene is measured using atomic force microscopy (AFM) (Figure 2c and 2d), which confirms the spherical-like shape. The CDs are negatively charged and therefore are unlikely to agglomerate in solution (further information about the characteristics of the CDs is presented in Figure S1).

Graphene and graphene-CDs devices were functionalized using 1-pyrenebutanoic acid succinimidyl ester (PBASE) linker for further CD63 antibody conjugation. PBASE stacks with graphene by π–π overlap to form a self-assembled monolayer with homogeneous coverage, while the N-hydroxysuccinimide (NHS) ester extends from the graphene surface to react with primary amines present on the antibodies. In order to confirm a good coverage of PBASE on the graphene surface, graphene samples were functionlized with PBASE at two different treatment times (2hr and 8hr). The samples were then analysed using XPS under the same conditions. As the density of PBASE is proportional to the number of nitrogen atoms in the PBASE, the N1s peak area was used as an indication of the PBASE coverage. The N1s peak was increased by an average of 11% when the PBASE treatment time was increased from 2hr to 8hr (Figure S2 and Table S1). Raman spectra of graphene after modification with PBASE show a strong increase in the disorder D peak at around 1350 cm^{-1} due to the resonance of sp^3 bonding[37] or due to localized vibrational modes of the PBASE interacting with extended phonon modes of graphene[38] (Figure 3a) (The I_D/I_G ratio extracted from the Raman map before and after PBASE modification is plotted in Figure S3). In addition, the presence of a one shoulder peak at 1380 cm^{-1} is attributed to disorder arising from orbital hybridization and another at 1616 cm^{-1} to a pyrene group resonance due to PBASE binding to the graphene surface.[37]

Specific antibodies were then conjugated to the PBASE immobilised surfaces. XPS demonstrated the presence of antibodies after conjugation. CD63 antibodies were selected to target CD63 markers on the surface of the exosomes. Using a commercial fluorescence kit, we confirmed that CD63 is a valid marker with abundant expression on the exosome surface and that the CD63 antibody exhibits a high capturing rate for this exosome (see supporting information Figures S5 and S6). The high-resolution N1s spectra show a significant increase in the N1s peak at 400.2 eV after CD63 conjugation (Figure 3b). The high-resolution C1s XPS spectrum reveals four components at the surface: C-C at 284.7 eV, C-O/C-N at 285.8 eV, C-O/C-N at 286.6, and O-C=O at 288.5 eV (Figure 3c), which can be attributed to the large number of amine and amide groups

present on the antibodies. The XPS spectra for the functionalization process for graphene and CDs-coated graphene are presented in Figure S4.

The surface morphology of graphene and graphene-CDs after each step of functionalization process was characterized using AFM (Figure 3d and 3e). The surface roughness of pristine graphene is extracted to be 0.25 nm. After 2hr PBASE treatment, surface roughness of graphene surface increased to 0.34 nm. Both ND-G and CDs-G show good coverage of CD63 antibody. The Ab density on graphene surface is extracted to be >2500 antibody/um^2 (Figure S7). The average size area of the antibody is extracted to be about 20±5 nm^2 after considering the convolution effect from AFM tip.

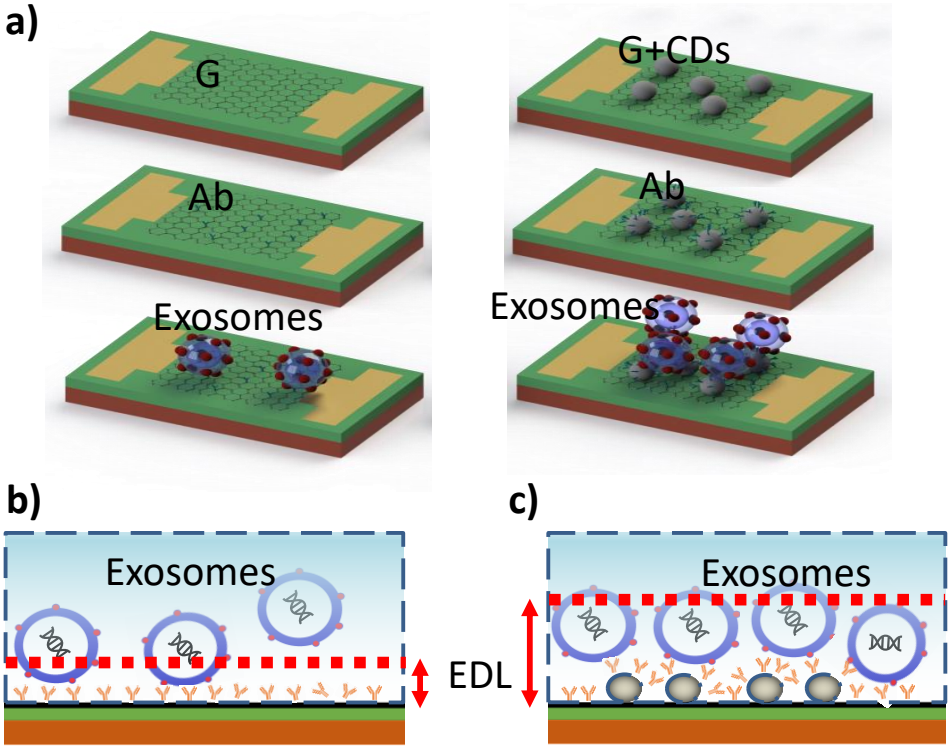

Figure 1. Schematic illustration of the GFET and CDs-GFET sensors. a) Device fabrication, surface modification and capturing of exosomes. G: graphene; CDs: carbon dots; Ab: antibodies. b) and c)

Schematic illustrations of the exosomes capture on (b) graphene and (c) CDs modified graphene. The decoration of CDs modifies the electrical double layer (EDL) and enhances capturing of exosome.

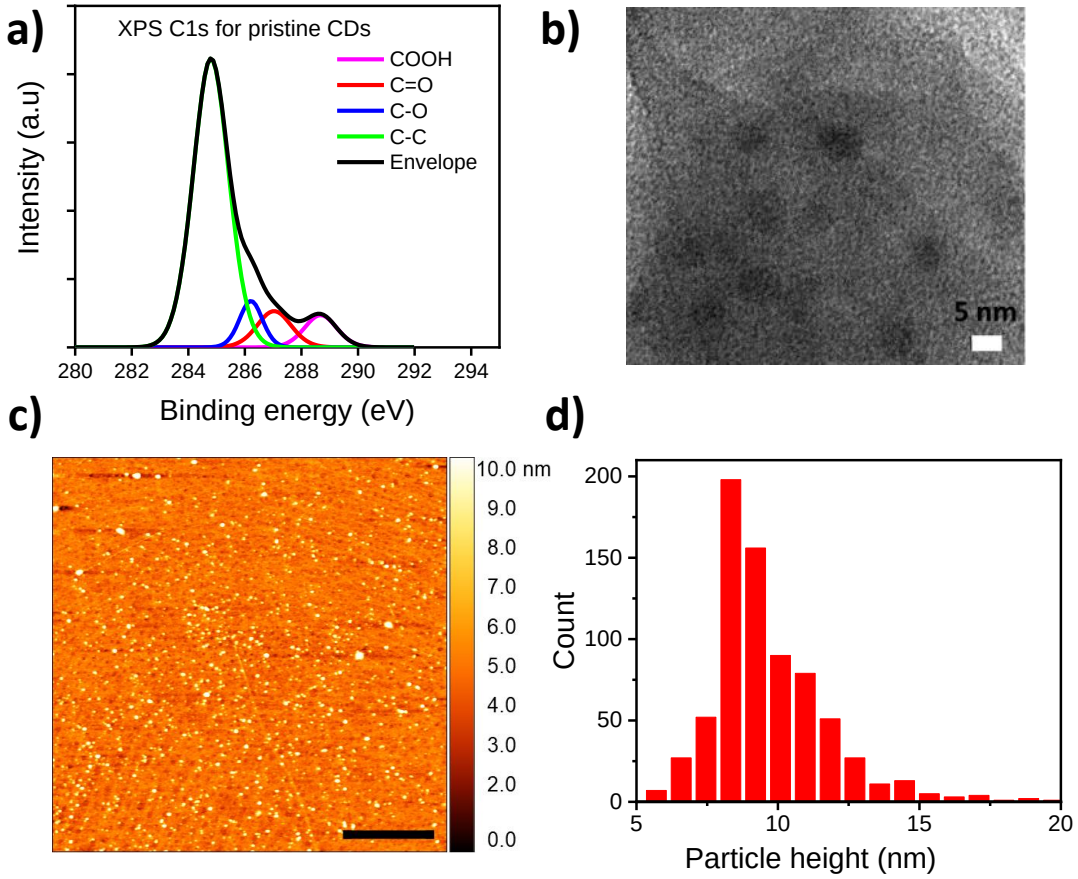

Figure 2. Characterisation of CDs and graphene surface fabrication. a) C1s XPS spectra of CDs. b) HRTEM image of CDs. Scale bar = 5 nm. c) AFM profile of CDs on graphene surface. Scale bars = 1 μm. d) histogram of CDs height distribution obtained from AFM.

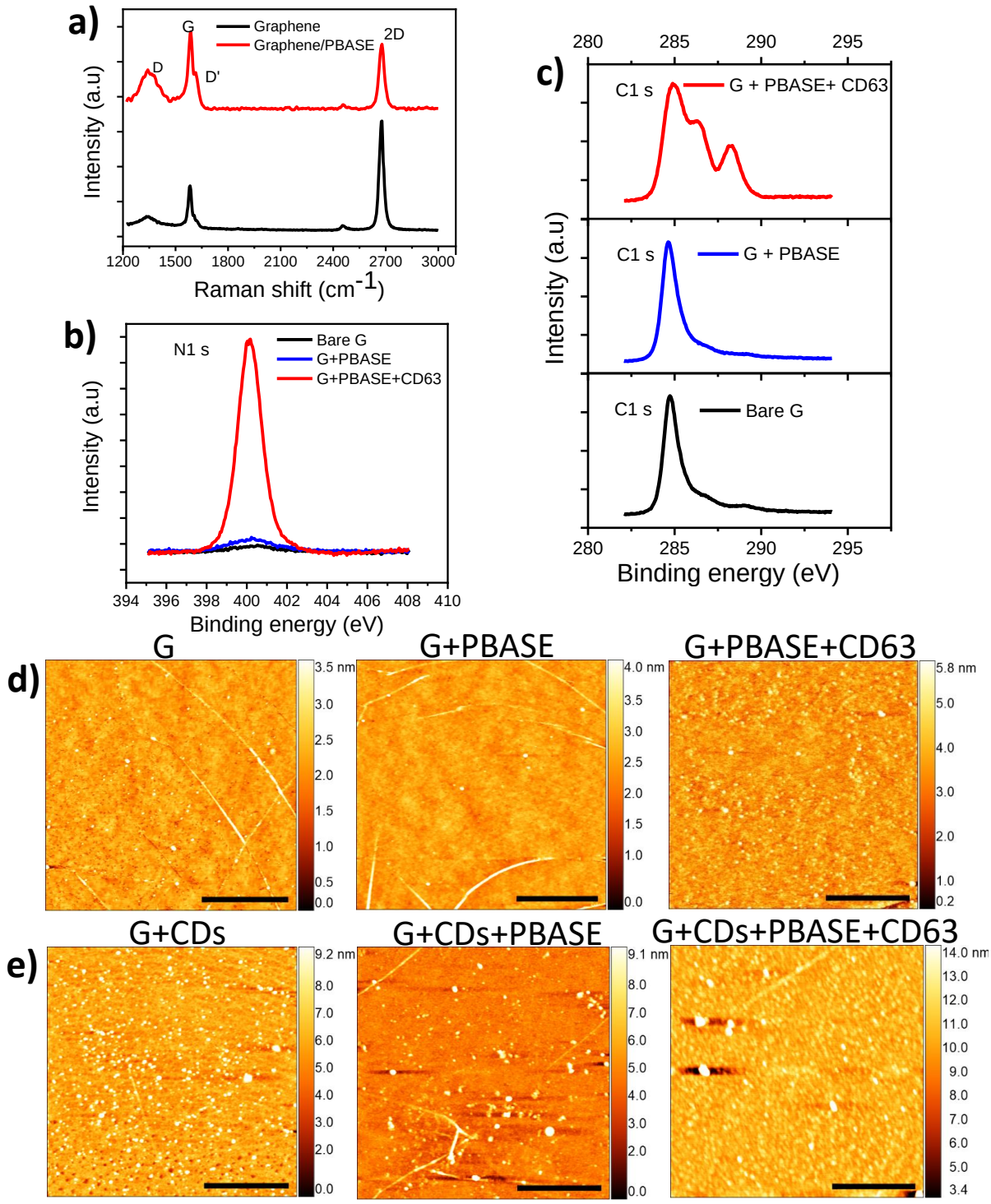

142

143 Figure 3. Characterization of surface functionalization of G and G-CDs. a) Raman spectra of bare graphene
144 and PBASE-functionalized graphene. b) N1s and (c) C1s XPS spectra of graphene with different levels of
145 functionalization: bare, with PBASE and with PBASE + CD63 antibody, respectively. d) AFM profiles of

bare G, after PBASE functionalization and Ab incubation. e) AFM profiles of CDs on G, after PBASE functionalization and Ab incubation. AFM scale bars = 1 μm.

After successful conjugation of antibodies, target exosomes were introduced to the CDs enhanced GFET sensors and plain GFET sensors for comparison. The electrical response of each device to exosomes was determined using liquid gates, i.e the source-drain current is measured as a function of the liquid gate voltage applied through a platinum wire. We first measured the stability of our devices in 1000 times diluted PBS with H_2O (0.001X PBS) after different rinsing times and change of Dirac voltage over time (Figure S9). The samples are stable in the buffer solution and relatively small drifts were observed over time. We further measured the hysteresis of a GFET sensor and CD-GFET sensor. The hysteresis was quantified by the voltage shift near the Dirac voltage, which was measured to be 10 mV and 11 mV for G-GFET sensor and CD-GFET sensor, respectively (Figure S10). GFET sensors are p-doped and the electron conduction is weaker than the hole conduction. This could be attributed to the difference in the scattering cross sections due to the electrostatic interaction of carriers in graphene with the charged impurities, which could be substrate impurities or impurities from the functionalized groups. [39-42] We performed transport measurements on non-functionalized graphene in solutions of different ionic strength to confirm the impact of impurity charges in the SiO_2 substrate underneath graphene. The symmetry and negative shift in Dirac point were observed with the increase in ionic strength where ions in the solution screen out the impurity charges[39] (Figure S11). Scattering of graphene carriers with the bonded antibodies and the pyrene linkers may be attributed to the asymmetry.[40, 42] After exosome binding the Dirac voltage is further positively shifted. The CDs-GFET sensors show a significant positive shift in the Dirac voltage after exosome binding compared with the pure graphene surface (Figure 4b, c). This is consistent with the effect of the negative charge of exosomes, which induces p-doping in graphene. A similar response was observed for a total of 8 devices (See Figure S12 for more device tests). The shift of the Dirac voltage shift as a function of exosome concentrations from 10 to 10^7 particles/μL is plotted in Figure 4d. This observation shows that CDs-GFET sensors have a value of sensitivity more than two orders of magnitude higher than that of a non-decorated (ND-GFET) sensors. By comparing the response from ND-GFET sensor and CDs-GFET sensor, we observed the ND-GFET sensor exhibits insiginificant response when the the concentration of exosomes is reduced below 10^4 particles/μL. On the other hand, a large shift in Dirac voltage is

observable at a concentration as low as 100 particles/μL for CDs-GFETs. Moreover, this value of the shift in Dirac point for CDs-GFET sensor is comparable to the shift measured in ND-GFET sensor at concentration as high as 10^5 particles/μL. Furthermore, the sensitivity of the GFETs sensor is increased from 15 mV/dec for ND-GFET sensor to 33 mV/dec for CDs-GFET sensor. This sensitivity of the sensor was calculated from the log-linear response (log(exosome concentration)-ΔV_D) in the linear region of the graph (Figure 4d). The limit of detection (LoD) was determined by blank signal (PBS) plus 3 standard deviations of the blank. The limit of detection of the proposed CD-GFET biosensor is among the lowest according to literatures on many other biosensors reported for exosome detection including electrical, electrochemical, or optical ones.[36, 43]

In order to investigate the specificity of ND-GFET sensor and CDs-GFET sensor, the surface of graphene was modified with a non-specific antibody instead of anti-CD63 Ab. The IgG1κ isotype control was conjugated after functionalisation of graphene surface with PBASE. The specific binding area of the IgG1κ isotype is different than that to the anti-CD63 antibody.Therefore, the target CD63 exosome membrane protein should not bind selectivity to the binding area of IgG1K isotype. The properties of funtionlized IgG1κ isotype on graphene surface are provided in the supporting information (AFM in Figure S8). Figure S13 shows the change in Dirac volage of isotype and anti-CD63 sensors for different concentrtions of exosomes. For both ND-GFET sensor and CDs-GFET sensor, there is small shift in Dirac volatage for isotype sensor compared with anti-CD63. This indicates that the target exosome binds specifically to anti-CD63. We further performed IV measurements to find out whether the exosome can non-selectively bind to CDs without CD63 Ab functionalization. CDs-GFET sensors without antibodies showed a negligible response compared with the ones functionalized with CD63 Ab (Figure S14). The observed small negative shift of the Dirac voltage indicates that only a very small number of exosomes (<10%) can bind non-selectively to CDs without specific antibodies.

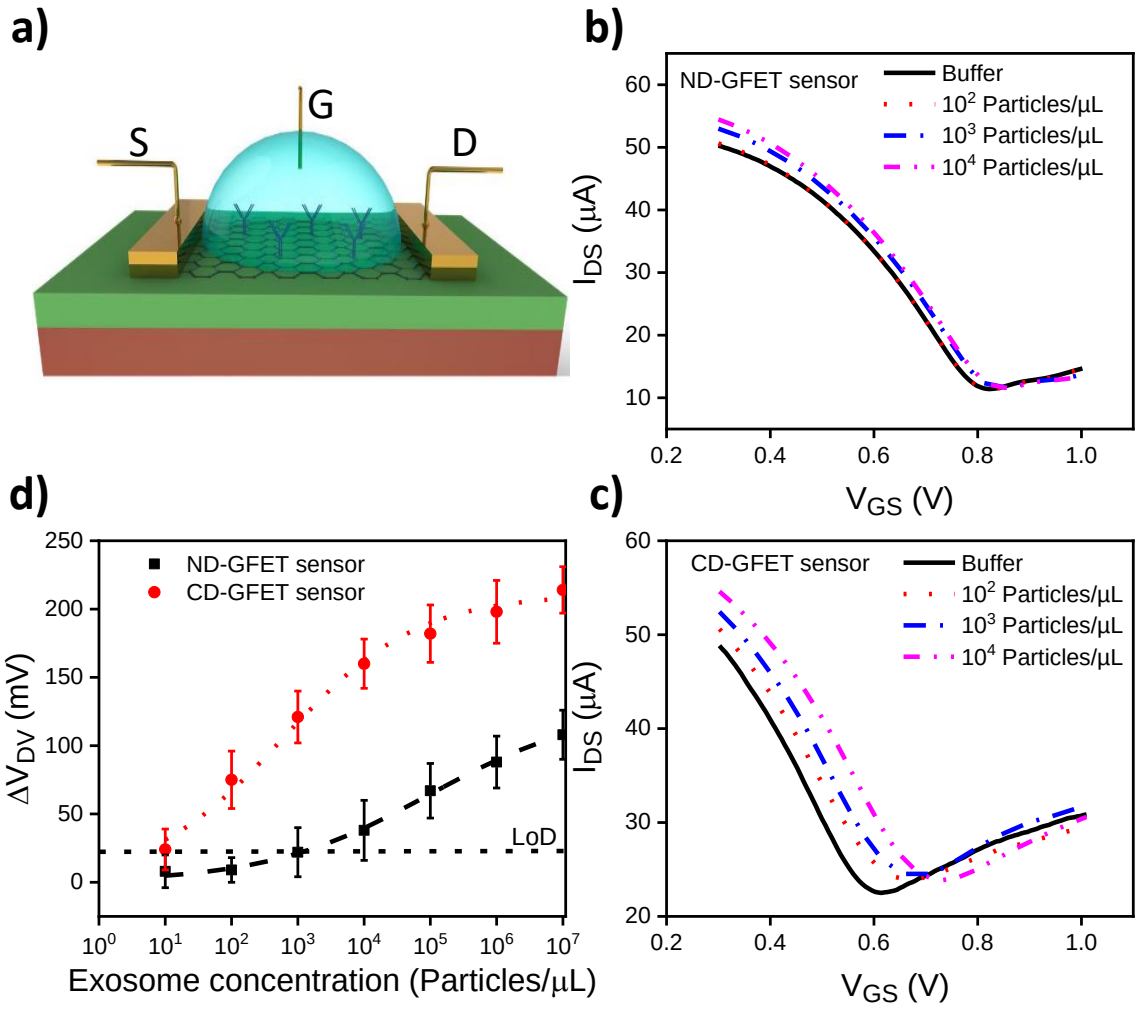

Figure 4. Electrical detection of exosomes on ND-GFET (non-decorated GFET) and CDs-GFET sensors. a) GFET sensor device structure showing source (S), drain (D) and top gate (G). Representative IDS-VGS curves of b) ND-GFET and c) CDs-GFET sensors after exosome binding. d) Dirac voltage shift of GFETs for various concentrations of exosomes on ND-GFET and CDs-GFET sensors (measurements were recorded after 15 mins of exosome incubation; error bars are determined by the standard deviation of multiple device measurements ($3 \leqslant n \leqslant 5$ for each reading)); (The baseline that represents LoD is defined by $(\text{response})_{PBS}$ + 3*standard deviation= 21 mV (n=5)).

Furthermore we measured the evolution of the sensor response as a function of time in order to evaluate the binding kinetics in both cases. The shift in Dirac voltage with time after exosome injection into the microfluidic channel is plotted in Figure 5. The results show that the response from graphene with CDs is faster than that from the non-decorated graphene surface, consistent with the explanation that CD-decorated surfaces capture more exosomes. Moreover, the Dirac voltage shift for CDs-GFETs rose quickly and reached saturation within 10 min, while that for the non-decorated GFETs shows a more linear response and takes longer to become saturated (See supporting information Table S3). Moreover, the shift from the GFET sensor doesn't reach the same level of shift as generated by CDs-GFET sensor.

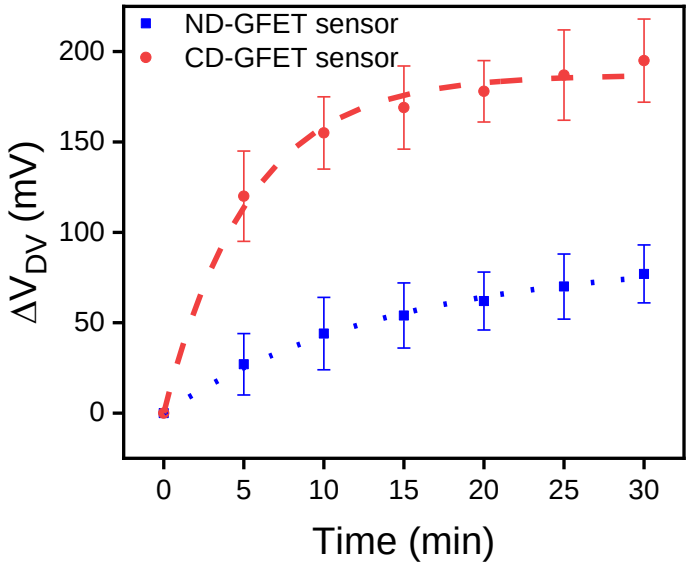

Figure 5. Evolution of Dirac voltage shift due to exosome binding as a function of time (n=3).

Microscopy imaging on labelled exosomes was further conducted to investigate the binding of exosomes to antibodies. Fluorescent exosomes were excited with evanescent wave (EW) illumination obtained from total internal reflection fluorescent (TIRF) microscopy. In order to reduce variation between samples, we modified half of the graphene surface on a cover slip with CDs while the other half was kept free from CDs before carrying out the rest of the functionalization process. Figure 6a,b shows the TIRF images of the dye labelled exosomes which appear as small fluorescent spots on the graphene surface with and without CDs modification.

(Note that again both surfaces were modified with CD63-binding antibodies according to our usual protocol, while exosome concentration used in this measurment was 10^8 particles/μL (see Methods). The exosome coverage is substantial in both cases, confirming that both CD-decorated and bare graphene surfaces have the potential to act as sensors. Quantification showed a 60% higher number of exosomes per unit area on the CD-decorated surface in comparison with the bare graphene surface (Figure 6c), supporting the concept that CD-decoration enhances exosome capture in this system. While carbon dots are weakly fluorescent in solution they are quenched when deposited due to aggregation-induced π-π stacking or resonance energy transfer (RET).[44] In our fluorescence imaging, there was no signal detected on a CD-only substrate. This demonstrates that the increase in fluorescence in Figure 6a,b is due to a significant increase in exosome concentration rather than the background.

While the TIRF measurements confirm the increase in exosome density on the CD-GFET surface, we carried out AFM scans in the same region of the CD-GFET before and after exosomes were added (Figure 7a,b) in order to check that the exosomes bind specifically to the CDs. The samples were incubated at room temperature for 20 min with an exosome concentration of 10^6 particles/μL. The incubation conditions were chosen such that a complete saturation of the graphene surface with exosomes was avoided. Based on a scanned area of 20 μm by 20 μm, we plotted a height histogram of around 90 particles. These particles were selected manually where CDs identified first, the change of particles height after exosome incubation was then measured. The statistical data shows an average increase in thickness of about 15 nm after exosome incubation (Figure 7c). The measured height is consistent with the height range of exosomes reported in the literature using AFM.[45-47] We then selected a spot of 5 μm X 5 μm and identified the exosome in that specific location both on CDs and graphene surfaces. Figure 7d shows that more than 70% of exosomes are attached to CDs surface, while only a few exosomes are attached to the graphene surface.

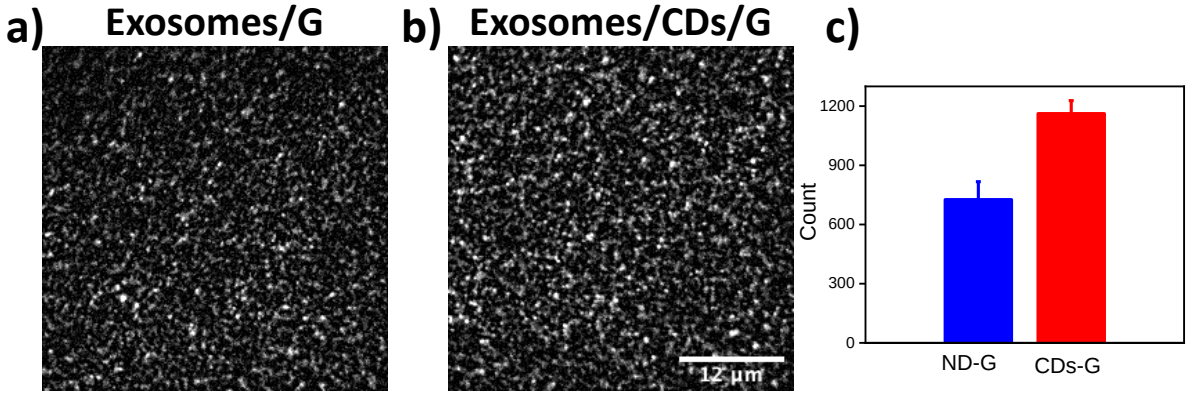

Figure 6. Comparison of exosomes captured on ND-GFET and CDs-GFET sensors: TIRF images captured on a) non-decorated graphene and b) CD-decorated graphene respectively (both surfaces were functionalized with anti-CD63); c) Exosomes count on ND-G and CDs-G taken from an average of 3 spots on the CD-decorated and 3 spots on the non-decorated grahene surface (for the full method of exosome counting see Methods).

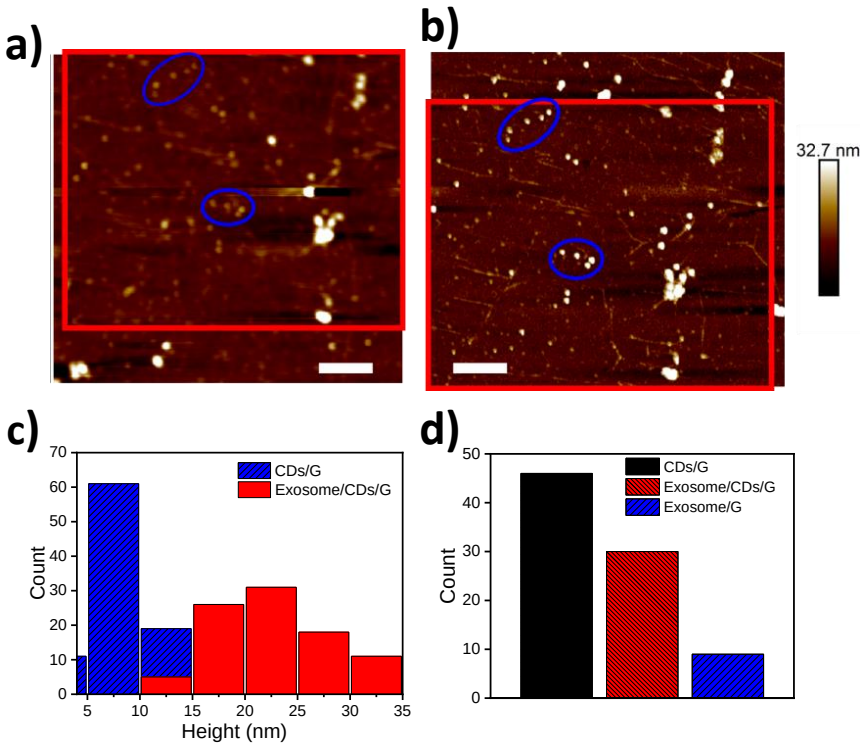

Figure 7. a) AFM profiles after CDs deposited on graphene, and b) after 20 min incubation of 106 exosomes/µL on functionalized CDs-GFETs surface (the same scanned region is highlighted in red); c) Histograms of height as measured by AFM of CDs before and after exosome incubation; d) count of number

of exosome captured on CDs-GFETs and bare GFETs surfaces (The data is taken from 5 μm X 5 μm spot). Scale bars: (a) and (b) 1 μm.

There are two possible mechanisms that could explain the enhanced sensor response with graphene decorated with CDs: geometry-enhanced capture rate in mass transport-reaction kinetics and reduced charged impurities through CDs. When considering transport-reaction kinetics, it appears that the geometry of CDs can significantly enhance the sensor response compared with flat graphene. Our data is supported by previous reports suggesting that the 3D geometry of sphere can largely enhance the diffusion transport of target molecules to the sensor surface due to the geometrical capacitance (See supporting information Section 6).[18, 27] The geometry of CDs can also enhance the reaction kinetics. The curvature and large surface area of nanosphere can facilitate a larger density of antibodies on nanospheres and increase the probability of multivalency interaction between antibodies and exosomes.[48, 49] The density of antibodies on graphene and CDs-G was investigated by comparing the intensity and area of N1s peak in XPS. We consistently observed an increase in the N1s peak intensity and area for CDs-G samples compared with ND-G (Figure 8). Based on 3 different samples and spot size of radius of 400 um, the average increase in N1s peak area of CDs-G was about 12.5% higher than ND-G. All measurements were done under the same conditions. This indicates the number of nitrogen atoms is higher for CDs-G samples and the density of antibody is higher on CDs-G samples.

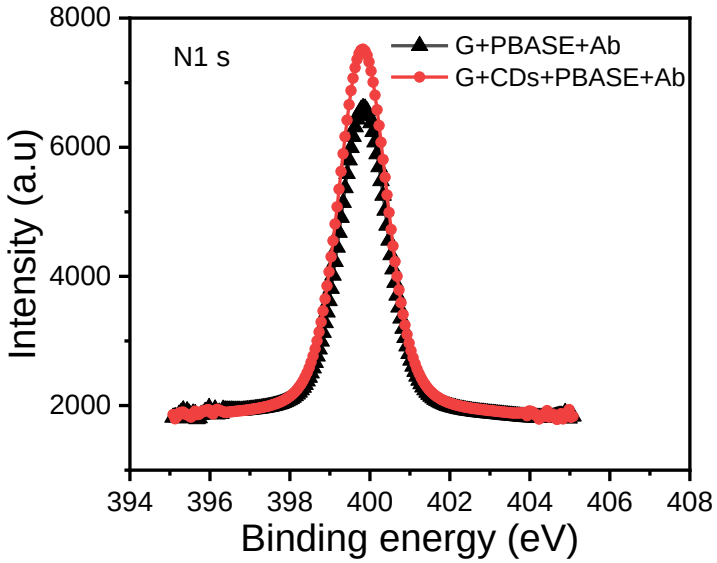

Figure 8. N1s XPS spectra of CD63 antibodies on PBASE functionalized graphene with and without carbon dot decoration (XPS spectra were recorded under the same conditions).

A second possible mechanism behind the sensitivity enhancement could be attributed to the increase in the effective charge of exosomes due to the modulation of electrical double layer capacitance. In order to investigate this hypothesis, we measured the interfacial capacitance of ND-G and CDs-G with the electrolyte (Figure 9). Using Cyclic-voltmmetry (CV), we observed a reduction in capacitance by a factor of 1.35-2.50 for CDs-G compared with ND-G. This decrease could be attributed to the increase in the Debye length or a decrease in dielectric constant. Since the conductivity of the GFETs is not significantly altered by the CDs, the effect of the dielectric constant is not expected to play a significant role. It has been reported that the electrostatic screening is weaker near a region of concave curvature in comparison to flat 16urfaces.[50] CDs can create concave curved areas near the interface to the graphene surface. We also observed that carbon dots improve the charge neutrality of graphene (Figure 4b,c and Figure S16), which could lead to an increase of the Debye length in similar way like a decrease of ionic strength.[7, 39] The reduction of the charge density can also reduce the quantum capacitance[51] by compensation of charged impurities in the SiO_2 surface – facilitated by functional groups attached to CDs. The latter may be most effective when the measurements are performed in buffer solution where the quantum capacitance C_Q is comparable to the double layer capacitance C_{dl}. We independently measured

double layer capacitance using a Pt electrode at the same conditions use for graphene measurements in order to quantify the effect of the quantum capacitance. The average value of C_{dl} is measured to be 3.52 μF/cm^2. This value is comparable to the extracted theoretical value of 3.10 μF/cm^2. We then extracted the average value of the quantum capacitance in ND-G from the total interfacial capacitance ($1/C_{dl} + 1/C_Q$) to be 8.68 μF/cm^2. The corresponding change in the induced surface potential due to exosome binding is inversely proportional to the interfacial capacitance: $\Delta V = \frac{-\Delta\sigma_{exo}}{C_{dl}+C_Q}$ where $\Delta\sigma_{exo}$ is the change in charge density by exosomes within the Debye length at the sensor surface. This explains the larger observed Dirac voltage shifts in CD-GFET in comparison to ND-FET sensors, assuming that both sensors have the same number of exosomes at their surfaces, due to lowering of its interfacial capacitance.

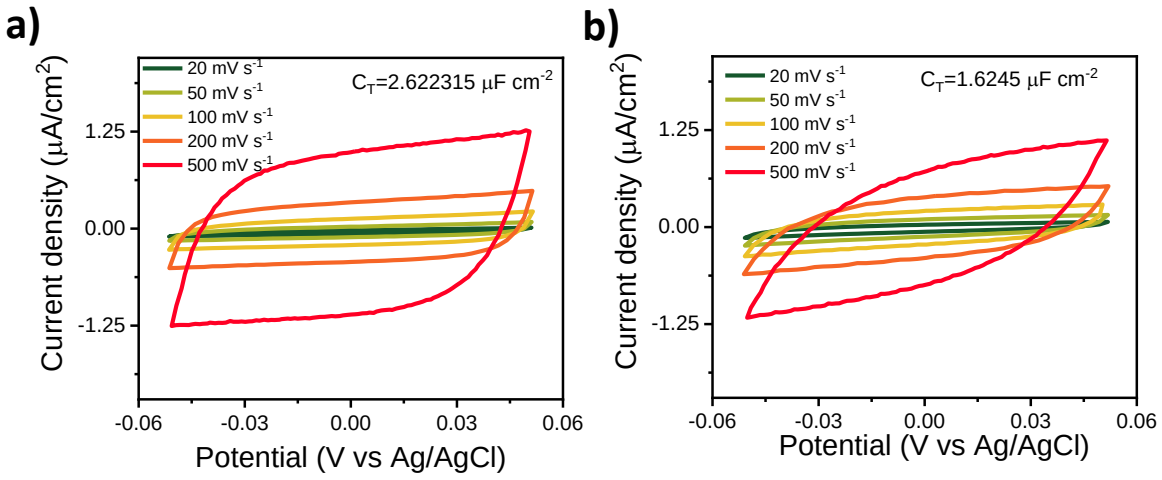

Figure 9. Capacitance measurements of a) ND graphene and b) CDs modified graphene. The reduction in EDL capacitance after CDs modification can lead to an increase of the Debye screening length.

Although there are some studies about deposited nanoparticles (NPs) like AuNPs an PtNPs on graphene to fabricate FET sensors,[52-55] these sensors do not fully exploit the capability of graphene sensors, rather than relying on the functionalization of NPs which makes the graphene surface largely unused.[52, 53] This can impact the sensitivity and selectivity of the graphene sensor. In contrast, we have demonstrated the functionalization of both graphene and CDs, resulting in a further increase of the sensitivity. In addition, most reported work with metallic nanoparticles on graphene is about DNA/miRNA detection, rather than the detection of targets of larger size such as exosomes. Therefore, our work is the first demonstration of a significant enhancement of GFET

sensitivity due to the deposition of CDs on graphene for sensing of exosomes. In addition, our process of depositing CDs on graphene surface relies on the simple incubation of a single droplet that contains CDs at room temperature for a few hours and does not require sophisticated systems such as two-chamber magnetron sputtering or colloidal systems to deposit NPs, which could add additional defects to the graphene.

3 Conclusion

In summary, we demonstrated a surface modification strategy to effectively improve the capture efficiency and sensitivity of graphene FET sensors by incorporating carbon dots on the graphene surface. The increase in capture rate can lead to an increase of the limit of detection by three orders of magnitude for GFET biosensors. LoD values down to 100 particles/μL of exosome detection were achieved by our experiments. The incorporation of carbon dots into graphene sensors is straightforward to form a compatible heterostructure without distorting the sp2 network of graphene. Therefore, our unique combination provides the advantage of fast capture and high capture efficiency through CDs with the unique intrinsic response of graphene, and is therefore expected to have a great potential for the development of high-performance biosensors for point-of-care early diagnosis of diseases.

4 Experimental Section

Preparation of Graphene Samples

Monolayer graphene grown by CVD on Cu foil was coated with poly(methyl methcrylate) (PMMA) to support the graphene transfer. Graphene at the backside of Cu foil was etched using oxygen plasma. The Cu was then etched using ammonium persulfate (APS) (0.01 g/mL in H_2O) overnight. The freestanding PMMA/graphene layer was transferred to a SiO_2/Si substrate. The PMMA/graphene on substrate was baked on a hotplate for 1 h at 150°C to improve the adhesion of graphene to the substrate. PMMA was then removed using acetone overnight followed by isopropanol (IPA) for 5 min. The sample was then annealed at 210°C for 16 h to remove PMMA residues on the graphene surface. The 10/50 nm Ti/Au electrodes were subsequently deposited by

DC magnetron sputtering for the FET source and drain electrodes. A polydimethylsiloxane (PDMS) channel (6 mm in length, 0.5 mm in width and height) was fabricated in-house and cured for 12 h at room temperature.

Preparation of CDs

A 10wt% solution of D-glucose in DI water underwent hydrothermal synthesis in a Teflon-lined stainless steel autoclave at 200 °C for 12 h. The resulting dark yellow solution was vacuum-filtered and subsequently dialysed for 72 h using a 1,000 Da regenerated cellulose membrane. The solution was freeze dried and the resulting powder was reconstituted to a concentration of 0.05 mg/mL as needed.

Modification of G-FETs Surface with CDs

CD water solution of 0.05 mg/mL was introduced to the graphene surface for 3-5 h before being rinsed with DI water and dried with N_2.

Functionalization and Antibody Conjugation

The FET samples were incubated for 2 h in PBASE 10 mM in dimethylformamide (DMF) (Sigma-Aldrich) at room temperature before being rinsed in DMF to remove excessive PBASE from the surface and dried with N_2. Following PBASE functionalisation, samples were conjugated with 100 μg/mL anti-CD63 antibody (BD Biosciences US). The CD63 antibodies are supplied in a stock solution of 0.5 mg/mL in an aqueous buffered solution (containing ≤0.09% sodium azide) and were diluted to 100 μg/mL using 1X PBS at pH 8.4. In order to conjugate these to PBASE NHS esters on the surface, FET sensors were incubated by placing a 25 μL droplet of the antibody solution onto the surface and left overnight in a humidified environment at 4°C. The sensors were then sequentially rinsed in 1X PBS at pH 8.4, de-ionised (DI) water and dried with N_2.

Raman Spectroscopy

Raman spectroscopy measurements were performed using a confocal Witec spectrometer and excited with laser wavelength of 532 nm (excitation energy $E_L = \hbar w_L = 2.33\ eV$) through an optical fibre, and an objective lens of 100X, NA=0.8 and laser spot of 0.4 μm. The laser power was kept below 2 mW and spectral resolution was ~3 cm^{-1}; the Raman peak position was calibrated

based on the Si peak position at 520.7 cm^{-1}. The D, G and 2D peaks were fitted with Lorenzian functions.

X-ray Photoelectron Spectroscopy (XPS)

XPS experiments and measurements were performed with K-Alpha+ and an Al radiation source ($hv = 1486.6\ eV$) in an ultrahigh vacuum chamber for spectroscopic analysis with a base pressure of 5×10^{-8} mbar.

Electrical Characterization

FET sensor measurements were performed in 0.001X PBS solution using a Keithley source meter. Source-drain voltage was fixed at 0.1 V and electrolyte gate was swept from 0 to 1.2 V at a sweeping rate of 0.03 VS^{-1}.

Purified exosomes from healthy plasma bought from HansaBioMed was used as a stock solution ($3 \text{ X } 10^{10}$ particles/mL). The working concentration of exosomes was prepared by a 10 times serial dilution from stock soluton. 1000 times diluted PBS was used as the solent.

Transmission Electron Microscopy (TEM) Measurements

High-resolution transmission electron microscopy (HRTEM) was used for CD imaging. The TEM images were taken with a JM21Plus HRTEM with an accelerating voltage of 200 kV.

Atomic Force Microscopy (AFM) Measurements

AFM was performed using Asylum MFP-3D classic and a Bruker Innova system in tapping mode with commercial tips of average radius 15 nm and typical scan resolution of 512 pixel X 512 pixel. All AFM scans were performed in dry conditions.

Total Internal Reflection Fluorescence (TIRF) Imaging

Sample preparation: After transfer onto a glass coverslip, the graphene was incubated for 2 h in PBASE (10 mM) in DMF at room temperature before being rinsed in DMF and dried with N_2. The sample surface was then conjugated with 50 μL of 0.1 mg/mL Alexa 568 labelled CD63 antibodies overnight in a humidified environment at 4°C. The CD63 antibodies (BD Biosciences) were pre-conjugated with Alexa 568 dye (Thermofisher, UK) according to the manufacturer' protocol and

extra unconjugated dye was removed by filtration with centrifuge at 12,000× g for 2 h with Amicon ultra 30 kDa cut-off filter. After antibody conjugation, the sample was then sequentially rinsed in 1× PBS at pH 8.4, DI water and dried in air or under N_2 flow. Similarly, isotype antibody (IgG1κ, BD Biosciences) was used for the preparation of the control sample. The GFP labelled exosomes (HansaBioMed) (50 μL, 0.01 mg/mL) were then added to the surface and incubated for 0.5 h. The sample was then rinsed with DI water and dried with N_2. TIRF measurements: The coverslip with sample was mounted onto a microscopic slide using nail polish. The sample was observed using total internal reflection fluorescence (TIRF) imaging carried out using a Leica TIRF microscope with 100× TIRF objective. Images were processed using the FIJI software package, using a central in-focus region of 250×250 pixels. A rolling ball background with 5 pixel rolling ball radius was subtracted. For quantification, exosomes were defined as locations of maxima in intensity using the procedure 'Find Maxima' with a 10% prominence threshold. The images presented have brightness and contrast adjusted for visual clarity, but quantification of exosomes was performed prior to this adjustment. The quoted increase in exosome density was determined from average values over 3 spots on the CD-decorated and 3 spots on the non-decorated surface. The exosome-counting approach is preferred to evaluate the total fluorescence signal as it will be less sensitive to variations in the apparent background fluorescence that may occur due to slight variations in TIRF angle and/or the graphene coupling to the surface.

Capacitance Measurements

The capacitance measurements of ND-G and CDs-G on 90nm(SiO_2)/Si(p++) substrate were carried out using a Methrom Multi Autolab/M101 with three electrodes setup, which consists of Ag/AgCl reference electrode, Pt rod counter electrode, and the surface of the graphene on silicon as the working electrode. While carrying out cyclic voltammetry (CV), all three electrodes were immersed in PBS solution for the measurement. The potential window was chosen between -0.05 V and 0.05 V due to minimum effect from the substrate.

ASSOSIATED CONTENT

Supporting Information.The Supporting information is available free of charge on the ACS Publications website at DOI:

Photoluminescence measurements of CDs, additional XPS, Raman and AFM of functionalization process, characterization of the exosomes and antibodies, Dirac voltage stability, hysteresis and ionic strength measurements, additional electrical tests of exosomes on ND-GFET and CD-GFET sensors, electrical measurements for isotype, electrical measurments for CD-GFET sensor without CD63 functionalization, electrical measurements of CDs under dry conditions, fitting models of the Dirac voltage measurements, diffusion model.

AUTHORS INFORMATION

Corresponding Authors

Sami Ramadan- Department of Materials, Imperial College London, South Kensington Campus, London SW7 2AZ, U.K. (ORCID: 0000-0002-0013-731X); Email: s.ramadan@imperial.ac.uk

Lizhou Xu- Department of Materials, Imperial College London, London, SW7 2AZ, UK. (ORCID: 0000-0001-5983-4059); Email: l.xu@imperial.ac.uk

Authors

Richard Lobo- Department of Chemical Engineering, Imperial College London, South Kensington Campus, London SW7 2AZ, U.K.

Yuanzhou Zhang- Department of Materials, Imperial College London, London, SW7 2AZ, UK.

Lizhou Xu- Department of Materials, Imperial College London, London, SW7 2AZ, UK. (ORCID: 0000-0001-5983-4059)

Olena Shaforost- Department of Materials, Imperial College London, London, SW7 2AZ, UK.

Deana Kwong Hong Tsang- Department of Materials, Imperial College London, London, SW7 2AZ, UK.

Jingyu Feng- Department of Chemical Engineering, Imperial College London, South Kensington Campus, London SW7 2AZ, U.K. (ORCID: 0000-0003-3181-4544)

Tianyi Yin- Department of Materials, Imperial College London, London, SW7 2AZ, UK.

Mo Qiao- Department of Chemical Engineering, Imperial College London, South Kensington Campus, London SW7 2AZ, U.K. (ORCID: 0000-0001-6354-7343)

Anvesh Rajeshirke- Department of Materials, Imperial College London, London, SW7 2AZ, UK.

Long R Jiao- Department of Hepatobiliary Surgery, Division of Surgery & Cancer, Imperial College London, Hammersmith Hospital Campus, Du Cane Road, London, W12 0NN, UK.

Peter K.Petrov- Department of Materials, Imperial College London, London, SW7 2AZ, UK. (ORCID: 0000-0003-3643-6685)

Iain E.Dunlop- Department of Materials, Imperial College London, London, SW7 2AZ, UK. (ORCID: 0000-0002-6329-4996)

Maria-Magdalena Titirici- Department of Chemical Engineering, Imperial College London, South Kensington Campus, London SW7 2AZ, U.K. (ORCID: 0000-0003-0773-2100)

Norbert Klein- Department of Materials, Imperial College London, London, SW7 2AZ, UK. (ORCID: 0000-0001-7854-8592)

Author Contributions

S.R., L.R.J., P.K.P., I.E.D., M.M.T., N.K. designed the study. SR., R.L., Y.Z., L.X., O.S., D.KHT., J. F., T.Y., M.Q., A.R., I.E.D. performed the experiments. SR., R.L., Y.Z., L.X., I.E.D analyzed the data. The manuscript was written through contributions of all authors.

ACKNOWLEDMENTS

This work was funded by UK's Engineering and Physical Science Research Council (EPSRC) through grant EP/P02985X/1. This work was partly supported by the Engineering and Physical Sciences Research Council (EPSRC) Reactive Plasmonics Programme (EP/M013812/1) and by the Henry Royce Institute through EPSRC grant EP/R00661X/1.

REFERENCES

1. Kaisti, M., Detection principles of biological and chemical FET sensors. *Biosensors and Bioelectronics* **2017,** *98*, 437-448.
2. Schedin, F.; Geim, A. K.; Morozov, S. V.; Hill, E. W.; Blake, P.; Katsnelson, M. I.; Novoselov, K. S., Detection of individual gas molecules adsorbed on graphene. *Nature Materials* **2007,** *6* (9), 652-655.
3. Sreeprasad, T. S.; Berry, V., How Do the Electrical Properties of Graphene Change with its Functionalization? *Small* **2013,** *9* (3), 341-350.
4. Kim, K. S.; Zhao, Y.; Jang, H.; Lee, S. Y.; Kim, J. M.; Kim, K. S.; Ahn, J.-H.; Kim, P.; Choi, J.-Y.; Hong, B. H., Large-scale pattern growth of graphene films for stretchable transparent electrodes. *Nature* **2009,** *457* (7230), 706-710.
5. Li, X.; Cai, W.; An, J.; Kim, S.; Nah, J.; Yang, D.; Piner, R.; Velamakanni, A.; Jung, I.; Tutuc, E.; Banerjee, S. K.; Colombo, L.; Ruoff, R. S., Large-Area Synthesis of High-Quality and Uniform Graphene Films on Copper Foils. *Science* **2009,** *324* (5932), 1312.
6. Campos, R.; Borme, J.; Guerreiro, J. R.; Machado, G.; Cerqueira, M. F.; Petrovykh, D. Y.; Alpuim, P., Attomolar Label-Free Detection of DNA Hybridization with Electrolyte-Gated Graphene Field-Effect Transistors. *ACS Sensors* **2019,** *4* (2), 286-293.
7. Hwang, M. T.; Heiranian, M.; Kim, Y.; You, S.; Leem, J.; Taqieddin, A.; Faramarzi, V.; Jing, Y.; Park, I.; van der Zande, A. M.; Nam, S.; Aluru, N. R.; Bashir, R., Ultrasensitive detection of nucleic acids using deformed graphene channel field effect biosensors. *Nature Communications* **2020,** *11* (1), 1543.
8. Andoy, N. M.; Filipiak, M. S.; Vetter, D.; Gutiérrez-Sanz, Ó.; Tarasov, A., Graphene-Based Electronic Immunosensor with Femtomolar Detection Limit in Whole Serum. *Advanced Materials Technologies* **2018,** *3* (12), 1800186.
9. Viswanathan, S.; Narayanan, T. N.; Aran, K.; Fink, K. D.; Paredes, J.; Ajayan, P. M.; Filipek, S.; Miszta, P.; Tekin, H. C.; Inci, F.; Demirci, U.; Li, P.; Bolotin, K. I.; Liepmann, D.; Renugopalakrishanan, V., Graphene–protein field effect biosensors: glucose sensing. *Materials Today* **2015,** *18* (9), 513-522.

10. Afsahi, S.; Lerner, M. B.; Goldstein, J. M.; Lee, J.; Tang, X.; Bagarozzi, D. A.; Pan, D.; Locascio, L.; Walker, A.; Barron, F.; Goldsmith, B. R., Novel graphene-based biosensor for early detection of Zika virus infection. *Biosensors and Bioelectronics* **2018,** *100*, 85-88.
11. Seo, G.; Lee, G.; Kim, M. J.; Baek, S.-H.; Choi, M.; Ku, K. B.; Lee, C.-S.; Jun, S.; Park, D.; Kim, H. G.; Kim, S.-J.; Lee, J.-O.; Kim, B. T.; Park, E. C.; Kim, S. I., Rapid Detection of COVID-19 Causative Virus (SARS-CoV-2) in Human Nasopharyngeal Swab Specimens Using Field-Effect Transistor-Based Biosensor. *ACS Nano* **2020,** *14* (4), 5135-5142.
12. Xu, L.; Li, D.; Ramadan, S.; Li, Y.; Klein, N., Facile biosensors for rapid detection of COVID-19. *Biosensors and Bioelectronics* **2020,** *170*, 112673.
13. Huang, Y.; Dong, X.; Liu, Y.; Li, L.-J.; Chen, P., Graphene-based biosensors for detection of bacteria and their metabolic activities. *Journal of Materials Chemistry* **2011,** *21* (33), 12358-12362.
14. Delle, L. E.; Pachauri, V.; Sharma, S.; Shaforost, O.; Ma, H.; Adabi, M.; Lilischkis, R.; Wagner, P.; Thoelen, R.; Klein, N.; O'Kennedy, R.; Ingebrandt, S., ScFv-modified graphene-coated IDE-arrays for 'label-free' screening of cardiovascular disease biomarkers in physiological saline. *Biosensors and Bioelectronics* **2018,** *102*, 574-581.
15. Zhou, L.; Wang, K.; Sun, H.; Zhao, S.; Chen, X.; Qian, D.; Mao, H.; Zhao, J., Novel Graphene Biosensor Based on the Functionalization of Multifunctional Nano-bovine Serum Albumin for the Highly Sensitive Detection of Cancer Biomarkers. *Nano-Micro Letters* **2019,** *11* (1), 20.
16. Fu, W.; Jiang, L.; van Geest, E. P.; Lima, L. M. C.; Schneider, G. F., Sensing at the Surface of Graphene Field-Effect Transistors. *Advanced Materials* **2017,** *29* (6), 1603610.
17. Kwong Hong Tsang, D.; Lieberthal, T. J.; Watts, C.; Dunlop, I. E.; Ramadan, S.; del Rio Hernandez, A. E.; Klein, N., Chemically Functionalised Graphene FET Biosensor for the Label-free Sensing of Exosomes. *Scientific Reports* **2019,** *9* (1), 13946.
18. Nair, P. R.; Alam, M. A., Performance limits of nanobiosensors. *Applied Physics Letters* **2006,** *88* (23), 233120.
19. Squires, T. M.; Messinger, R. J.; Manalis, S. R., Making it stick: convection, reaction and diffusion in surface-based biosensors. *Nature Biotechnology* **2008,** *26* (4), 417-426.
20. Kwon, S. S.; Choi, J.; Heiranian, M.; Kim, Y.; Chang, W. J.; Knapp, P. M.; Wang, M. C.; Kim, J. M.; Aluru, N. R.; Park, W. I.; Nam, S., Electrical Double Layer of Supported Atomically Thin Materials. *Nano Letters* **2019,** *19* (7), 4588-4593.
21. Zou, X.; Wei, S.; Jasensky, J.; Xiao, M.; Wang, Q.; Brooks, C. L.; Chen, Z., Molecular Interactions between Graphene and Biological Molecules. *Journal of the American Chemical Society* **2017,** *139* (5), 1928-1936.
22. Wei, S.; Zou, X.; Tian, J.; Huang, H.; Guo, W.; Chen, Z., Control of Protein Conformation and Orientation on Graphene. *Journal of the American Chemical Society* **2019,** *141* (51), 20335-20343.
23. Poortinga, A. T.; Bos, R.; Norde, W.; Busscher, H. J., Electric double layer interactions in bacterial adhesion to surfaces. *Surface Science Reports* **2002,** *47* (1), 1-32.
24. Norde, W.; Lyklema, J., Why proteins prefer interfaces. *Journal of Biomaterials Science, Polymer Edition* **1991,** *2* (3), 183-202.
25. Soleymani, L.; Fang, Z.; Sargent, E. H.; Kelley, S. O., Programming the detection limits of biosensors through controlled nanostructuring. *Nature Nanotechnology* **2009,** *4* (12), 844-848.
26. Soleymani, L.; Fang, Z.; Lam, B.; Bin, X.; Vasilyeva, E.; Ross, A. J.; Sargent, E. H.; Kelley, S. O., Hierarchical Nanotextured Microelectrodes Overcome the Molecular Transport Barrier To Achieve Rapid, Direct Bacterial Detection. *ACS Nano* **2011,** *5* (4), 3360-3366.
27. Kim, B.-Y.; Sohn, I.-y.; Lee, D.; Han, G. S.; Lee, W.-I.; Jung, H. S.; Lee, N.-E., Ultrarapid and ultrasensitive electrical detection of proteins in a three-dimensional biosensor with high capture efficiency. *Nanoscale* **2015,** *7* (21), 9844-9851.

28. Gao, X.; Ding, C.; Zhu, A.; Tian, Y., Carbon-Dot-Based Ratiometric Fluorescent Probe for Imaging and Biosensing of Superoxide Anion in Live Cells. *Analytical Chemistry* **2014,** *86* (14), 7071-7078.
29. Yuan, F.; Li, S.; Fan, Z.; Meng, X.; Fan, L.; Yang, S., Shining carbon dots: Synthesis and biomedical and optoelectronic applications. *Nano Today* **2016,** *11* (5), 565-586.
30. Baker, S. N.; Baker, G. A., Luminescent Carbon Nanodots: Emergent Nanolights. *Angewandte Chemie International Edition* **2010,** *49* (38), 6726-6744.
31. Luo, H.; Papaioannou, N.; Salvadori, E.; Roessler, M. M.; Ploenes, G.; van Eck, E. R. H.; Tanase, L. C.; Feng, J.; Sun, Y.; Yang, Y.; Danaie, M.; Belen Jorge, A.; Sapelkin, A.; Durrant, J.; Dimitrov, S. D.; Titirici, M.-M., Manipulating the Optical Properties of Carbon Dots by Fine-Tuning their Structural Features. *ChemSusChem* **2019,** *12* (19), 4432-4441.
32. Yan, F.; Jiang, Y.; Sun, X.; Bai, Z.; Zhang, Y.; Zhou, X., Surface modification and chemical functionalization of carbon dots: a review. *Microchimica Acta* **2018,** *185* (9), 424.
33. Essner, J. B.; Baker, G. A., The emerging roles of carbon dots in solar photovoltaics: a critical review. *Environmental Science: Nano* **2017,** *4* (6), 1216-1263.
34. Kalluri, R.; LeBleu, V. S., The biology, function, and biomedical applications of exosomes. *Science* **2020,** *367* (6478), eaau6977.
35. Melo, S. A.; Luecke, L. B.; Kahlert, C.; Fernandez, A. F.; Gammon, S. T.; Kaye, J.; LeBleu, V. S.; Mittendorf, E. A.; Weitz, J.; Rahbari, N.; Reissfelder, C.; Pilarsky, C.; Fraga, M. F.; Piwnica-Worms, D.; Kalluri, R., Glypican-1 identifies cancer exosomes and detects early pancreatic cancer. *Nature* **2015,** *523* (7559), 177-182.
36. Xu, L.; Shoaie, N.; Jahanpeyma, F.; Zhao, J.; Azimzadeh, M.; Al–Jamal, K. T., Optical, electrochemical and electrical (nano)biosensors for detection of exosomes: A comprehensive overview. *Biosensors and Bioelectronics* **2020,** *161*, 112222.
37. Liu, Y.; Yuan, L.; Yang, M.; Zheng, Y.; Li, L.; Gao, L.; Nerngchamnong, N.; Nai, C. T.; Sangeeth, C. S. S.; Feng, Y. P.; Nijhuis, C. A.; Loh, K. P., Giant enhancement in vertical conductivity of stacked CVD graphene sheets by self-assembled molecular layers. *Nature Communications* **2014,** *5* (1), 5461.
38. Wang, S.; Hossain, M. Z.; Shinozuka, K.; Shimizu, N.; Kitada, S.; Suzuki, T.; Ichige, R.; Kuwana, A.; Kobayashi, H., Graphene field-effect transistor biosensor for detection of biotin with ultrahigh sensitivity and specificity. *Biosensors and Bioelectronics* **2020,** *165*, 112363.
39. Chen, F.; Xia, J.; Tao, N., Ionic Screening of Charged-Impurity Scattering in Graphene. *Nano Letters* **2009,** *9* (4), 1621-1625.
40. Woo, S. O.; Froberg, J.; Pan, Y.; Tani, S.; Goldsmith, B. R.; Yang, Z.; Choi, Y., Protein Detection Using Quadratic Fit Analysis near the Dirac Point of Graphene Field-Effect Biosensors. *ACS Applied Electronic Materials* **2020,** *2* (4), 913-919.
41. Srivastava, P. K.; Arya, S.; Kumar, S.; Ghosh, S., Relativistic nature of carriers: Origin of electron-hole conduction asymmetry in monolayer graphene. *Physical Review B* **2017,** *96* (24), 241407.
42. Hayasaka, T.; Lin, A.; Copa, V. C.; Lopez, L. P.; Loberternos, R. A.; Ballesteros, L. I. M.; Kubota, Y.; Liu, Y.; Salvador, A. A.; Lin, L., An electronic nose using a single graphene FET and machine learning for water, methanol, and ethanol. *Microsystems & Nanoengineering* **2020,** *6* (1), 50.
43. Yu, Y.; Li, Y.-T.; Jin, D.; Yang, F.; Wu, D.; Xiao, M.-M.; Zhang, H.; Zhang, Z.-Y.; Zhang, G.-J., Electrical and Label-Free Quantification of Exosomes with a Reduced Graphene Oxide Field Effect Transistor Biosensor. *Analytical Chemistry* **2019,** *91* (16), 10679-10686.
44. Chen, Y.; Zheng, M.; Xiao, Y.; Dong, H.; Zhang, H.; Zhuang, J.; Hu, H.; Lei, B.; Liu, Y., A Self-Quenching-Resistant Carbon-Dot Powder with Tunable Solid-State Fluorescence and Construction of Dual-Fluorescence Morphologies for White Light-Emission. *Advanced Materials* **2016,** *28* (2), 312-318.

45. Parisse, P.; Rago, I.; Ulloa Severino, L.; Perissinotto, F.; Ambrosetti, E.; Paoletti, P.; Ricci, M.; Beltrami, A. P.; Cesselli, D.; Casalis, L., Atomic force microscopy analysis of extracellular vesicles. *European Biophysics Journal* **2017,** *46* (8), 813-820.
46. Sharma, S.; Gillespie, B. M.; Palanisamy, V.; Gimzewski, J. K., Quantitative Nanostructural and Single-Molecule Force Spectroscopy Biomolecular Analysis of Human-Saliva-Derived Exosomes. *Langmuir* **2011,** *27* (23), 14394-14400.
47. Sebaihi, N.; De Boeck, B.; Yuana, Y.; Nieuwland, R.; Pétry, J., Dimensional characterization of extracellular vesicles using atomic force microscopy. *Measurement Science and Technology* **2017,** *28* (3), 034006.
48. De Luna, P.; Mahshid, S. S.; Das, J.; Luan, B.; Sargent, E. H.; Kelley, S. O.; Zhou, R., High-Curvature Nanostructuring Enhances Probe Display for Biomolecular Detection. *Nano Letters* **2017,** *17* (2), 1289-1295.
49. Rutten, I.; Daems, D.; Lammertyn, J., Boosting biomolecular interactions through DNA origami nano-tailored biosensing interfaces. *Journal of Materials Chemistry B* **2020,** *8* (16), 3606-3615.
50. Shoorideh, K.; Chui, C. O., On the origin of enhanced sensitivity in nanoscale FET-based biosensors. *Proceedings of the National Academy of Sciences* **2014,** *111* (14), 5111.
51. Xia, J.; Chen, F.; Li, J.; Tao, N., Measurement of the quantum capacitance of graphene. *Nature Nanotechnology* **2009,** *4* (8), 505-509.
52. Danielson, E.; Sontakke, V. A.; Porkovich, A. J.; Wang, Z.; Kumar, P.; Ziadi, Z.; Yokobayashi, Y.; Sowwan, M., Graphene based field-effect transistor biosensors functionalized using gas-phase synthesized gold nanoparticles. *Sensors and Actuators B: Chemical* **2020,** *320*, 128432.
53. Cai, B.; Huang, L.; Zhang, H.; Sun, Z.; Zhang, Z.; Zhang, G.-J., Gold nanoparticles-decorated graphene field-effect transistor biosensor for femtomolar MicroRNA detection. *Biosensors and Bioelectronics* **2015,** *74*, 329-334.
54. Yin, Z.; He, Q.; Huang, X.; Zhang, J.; Wu, S.; Chen, P.; Lu, G.; Chen, P.; Zhang, Q.; Yan, Q.; Zhang, H., Real-time DNA detection using Pt nanoparticle-decorated reduced graphene oxide field-effect transistors. *Nanoscale* **2012,** *4* (1), 293-297.
55. Wang, S.; Hossain, M. Z.; Han, T.; Shinozuka, K.; Suzuki, T.; Kuwana, A.; Kobayashi, H., Avidin–Biotin Technology in Gold Nanoparticle-Decorated Graphene Field Effect Transistors for Detection of Biotinylated Macromolecules with Ultrahigh Sensitivity and Specificity. *ACS Omega* **2020,** *5* (46), 30037-30046.

641 **Table of Content (ToC) Graphics**

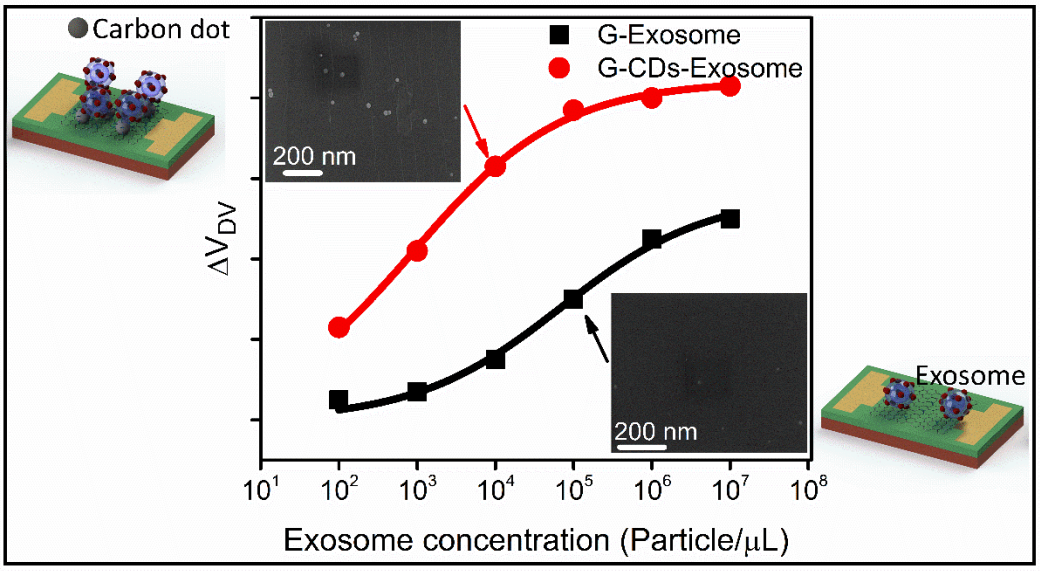

642